Estimating posture-recognition performance in sensing garments using geometric wrinkle modeling

Estimating Posture-Recognition Performance in Sensing Garments Using Geometric Wrinkle Modeling

Holger Harms, Oliver Amft, and Gerhard Tröster, *Senior Member, IEEE*

***Abstract*—A fundamental challenge limiting information quality obtained from smart sensing garments is the influence of textile movement relative to limbs. We present and validate a comprehensive modeling and simulation framework to predict recognition performance in casual loose-fitting garments. A statistical posture and wrinkle-modeling approach is introduced to simulate sensor orientation errors pertained to local garment wrinkles. A metric was derived to assess fitting, the body-garment mobility. We validated our approach by analyzing simulations of shoulder and elbow rehabilitation postures with respect to experimental data using actual casual garments. Results confirmed congruent performance trends with estimation errors below 4% for all study participants. Our approach allows to estimate the impact of fitting before implementing a garment and performing evaluation studies with it. These simulations revealed critical design parameters for garment prototyping, related to performed body posture, utilized sensing modalities, and garment fitting. We concluded that our modeling approach can substantially expedite design and development of smart garments through early-stage performance analysis.**

***Index Terms*—Smart garments, SMASH, system performance, wearable computers, wearable sensors.**

I. Introduction

MOVEMENT and posture monitoring using body-worn inertial sensors was found beneficial for out-of-lab, real-life assistive systems in different fields, including sports monitoring and movement rehabilitation [1], [2]. Recent advances in technology miniaturization allows integration of inertial sensors and monitoring functionality into textiles and to create smart sensing garments, e.g., the SMArt SHirt (SMASH) [3]. Eventually, these monitoring garments could enable new on-body assistance solutions, such as emergency systems for patients and the elderly [4], [5], personal sport coaches [6], and at-home training assistants in movement rehabilitation [7], [8].

Robustness in derived information and wearer acceptance are essential, but often contradictory requirements for such monitoring garments. Wearer acceptance typically requires unobtrusive, fashionable garments that can be conveniently worn, attached, and removed. In contrast, information robustness is hampered by casual cut, plainly the "looseness" of a garment, where sensors could pick up relative movements between garment and body. Accordingly, sensors incur orientation errors and deliver deteriorated information quality, e.g., observed as reduced posture-recognition performance [9]. Misalignment and movement of sensors is a frequently occurring issue in body-worn system design and in particular smart garments. The problem can be broadly eliminated by tight fitting, as it is frequently done in rehabilitation applications [7], [10], [11]. However, this approach is not viable in fields including home rehabilitation, where handicapped users often perceive difficulties in attaching normal casual clothes. In addition, movement rehabilitation benefits from monitoring joint movement at high resolution [8], [12]. Consequently, orientation errors need to be accounted for in garment design and application at an early stage. While investigations of orientation errors were made regarding elimination on signal [13] and recognition level [14], to our knowledge, there is no explicit simulative analysis of orientation errors in garment-attached sensors.

The challenge to estimate garment-related orientation errors at the human skin is related to a variety of factors that influence textile drape. These include current and past postures of the wearer, body proportions, fabric material properties, and external factors, such as humidity, friction, and air movement [15], [16]. Considering the variety of factors affecting textile drape, its nonstationary, nonlinear, and anisotropic behavior [17], it was found intractable to approach a precise physical garment simulation [18]. Thus, garment wrinkle structure and resulting effects on sensor information quality are not sufficiently understood. Nevertheless, design, sensor choice, and signal processing in smart garments require to systematically account for garment fit and consequently for orientation errors originating from textile wrinkles.

This paper introduces and validates a comprehensive framework to simulate garment-based sensor orientation errors (SOEs) and to estimate system performance in rehabilitation applications. Our approach pioneers in describing structure and outline of textile wrinkles related to a metric quantifying garment–skin fitting, which we call *body-garment mobility* (BGM). Using wrinkle descriptions, we simulate its statistical effect on sensor-orientation and posture-recognition performance. Given a posture set, our framework allows estimation of the required garment fitting for a particular recognition performance. In addition, it enables us to explore benefits of alternative and additional sensor modalities before actually

Manuscript received June 30, 2010; revised August 22, 2010; accepted August 22, 2010. Date of publication September 27, 2010; date of current version November 5, 2010.

H. Harms and G. Tröster are with the Wearable Computing Laboratory, Eidgenössische Technische Hochschule Zürich (ETH Zürich), CH-8092 Zürich, Switzerland (e-mail: harms@ieee.org; troester@ife.ee.ethz.ch).

O. Amft is with the ETH Zürich, Wearable Computing Laboratory, CH-8092 Zürich, Switzerland, and also with the ACTLab, Signal Processing Systems, Technische Universiteit (TU) Einhoven, NL-5600 MB Eindhoven, The Netherlands (e-mail: amft@ieee.org).

Color versions of one or more of the figures in this paper are available online at http://ieeexplore.ieee.org.

Digital Object Identifier 10.1109/TITB.2010.2076822

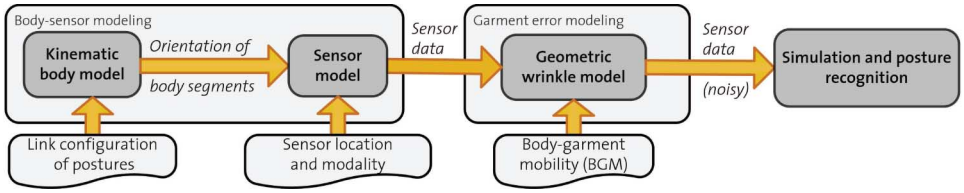

Fig. 1. Outline of our simulation framework: 1) kinematic body model using parametric descriptions of postures to derive body-segment orientation; 2) sensor model to simulate sensor readings of arbitrary inertial modalities; 3) geometric wrinkle model to estimate SOEs, as they occur in worn garments; and 4) recognition simulation to estimate the influence of orientation errors on posture discrimination.

implementing them into a garment and performing participant evaluation studies.

The proposed simulation framework was subsequently validated by comparing performance estimations to experimental study recordings from five participants using the SMASH prototyping garment [3].

Specifically, this paper makes the following contributions:

1) We introduce a configurable modeling and simulation approach to describe natural human postures, derive readings of body-worn inertial sensors, and simulate orientation errors depending on the BGM metric. Postures of shoulder and arm rehabilitation exercises are utilized to demonstrate versatility of our modeling approach.
2) We present a geometric wrinkle model to describe SOEs statistically. It enables our analysis and simulation of garment-orientation impact.
3) We provide simulation results for rehabilitation posture-recognition performances to a) validate our modeling approach with respect to empirical recordings; b) analyze effects of garment fitting using BGM; and (c) estimate benefits of different sensor modalities and locations.

In our earlier study, we compared rehabilitation posture recognition between garment and skin-attached sensors and observed an average recognition performance reduction of 13% [9] for 21 postures. Moreover, we performed simulations using a body model and empirically sampled textile orientation errors to analyze orientation errors and found that the performance deterioration of posture classification can be described [19]. However, due to the empirical error estimation, this approach was constrained to the observed conditions. Our current study profoundly extends on these initial results, as a complete parameterizable modeling framework is introduced to categorize and quantify orientation errors, validated by empirical data.

II. Modeling and Simulation Framework

Our study aims to systematically evaluate the influence of textile wrinkles on sensor orientation, and subsequent rehabilitation posture recognition for inertial sensors in smart garments. Due to the hard predictability problem of drape in textiles and garment movement, a full physical shape and alignment simulation has been found unfeasible. Instead, we focus on deriving a local statistical garment error model that considers BGM and permits prediction of local sensor orientation errors. We employ a theoretical framework of body and sensor models, which—in combination with garment error model—provide statistical orientation errors under the influence of local garment wrinkles.

As the performance of smart garments in rehabilitation-posture-monitoring applications depend on several design aspects, we structured our approach in a modular, configurable architecture, illustrated in Fig. 1. Our framework consists of the following modules.

1) *Kinematic body model:* Number and characteristics of the posture set that a garment should monitor influences discrimination performance. This module translates parametric descriptions of arbitrary postures into the orientation of body-model segments. The model is configured using relative angles between body segments. In this study, we concentrate on a specific set of postures used in shoulder rehabilitation (see Section III).
2) *Sensor model:* Type and complexity of sensors can vary from acceleration to attitude heading reference systems, which provide complete orientation information. This module transforms body-segment orientation of the kinematic body model into output of different sensor modalities (see Section III). The sensor model is configured by placement and modality parameters. In this study, we consider acceleration, and earth magnetic field measurement units attached to the upper limbs.
3) *Geometric wrinkle model:* BGM is related to SOEs, and thus to system performance. This module is used to describe the local sensor orientation with respect to BGM using a geometric textile curvature modeling approach. Statistics of the induced orientation errors are derived from this model and modulated on sensor data to perform simulations (see Section IV).
4) *Simulation and posture recognition:* The combined model effects can be efficiently analyzed using simulations. This module is dedicated to evaluate posture-recognition performance on the basis of modeled postures, sensor positions, modalities, and BGM. In this study, we evaluate the influence of these individual parameters and validate recognition performance of the complete framework (see Sections V and VI).

III. Body-Sensor Modeling

The body-sensor model contains two submodules. A kinematic body model is used to provide body-segment orientation according to parametric posture descriptions. The body-segment orientation is subsequently utilized by a sensor model to simulate the output of inertial sensors.

TABLE I
DENAVIT–HARTENBERG PARAMETER FOR $n = 7$ LINKS SPECIFYING A SERIAL-LINK MANIPULATOR FOR THE RIGHT BODY SIDE

$Link$ n	α_n $[rad]$	r_n $[mm]$	θ_n $[rad]$	d_n $[mm]$	Functional motion
1	0	180[a]	0	0	N/A
2	$\pi/2$	0	0	0	Shoulder extension
3	0	0	$-\pi/2$	0	Shoulder abduction
4	$-\pi/2$	0	0	0	N/A
5	$\pi/2$	0	0	-280[b]	Shoulder int. rotation
6	$-\pi/2$	0	0	0	Elbow flexion
7	0	0	0	-260[c]	Forearm pronation

Parameters according to [22]: [a] length of collarbone; [b] length of upper arm; [c] length of forearm.

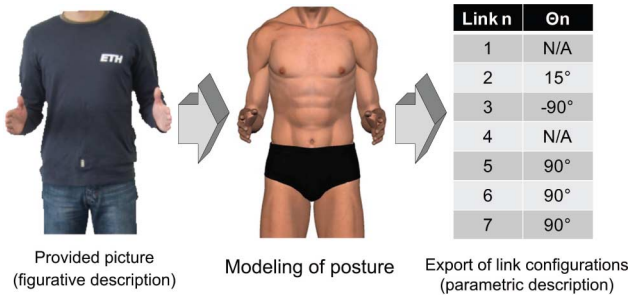

Fig. 2. Illustration of the posture modeling approach. Actual posture pictures (left) were reproduced using a *Poser* avatar (middle). Subsequently, joint angles, represented by link configurations, were extracted for a kinematic body model (right).

A. Kinematic Body Model

A parametric description of body and arm postures is derived by decomposing the upper body into serially linked segments according to human anatomic structures. A serial-link manipulator is formed, where each two segments are connected by a joint with one or more rotational degrees of freedom. Subsequently, body postures are described by a relative configuration of the segments, expressed as joint angles.

Computation of position and orientation of a serial-link manipulator in world coordinates is a forward-kinematics problem, where homogeneous transformation matrices can be used to describe links from serial segments [20]. The minimal form of these transformation matrices is given by four Denavit–Hartenberg (D–H) parameters [21]: 1) length r_i of the link (derived from anatomy); 2) twist α_i of the link (derived from anatomy); 3) offset d_i, denoting the relative link length; and 4) angle θ, denoting the inclination of a rotational joint. In this study, parameter d_i is treated as fixed, and θ as configurable.

Left and right body sides were obtained by two independent kinematic chains of seven links. Table I specifies the D–H parameter set used for the right upper body side. Our link representation allows for 5 DOF in each manipulator, which is sufficient to describe elbow and shoulder movements. Physical dimensions of links, which represent limb segments, were assumed according to standardized anthropometric measures of man (20–65 years, 78.4 kg) [22].

We described upper body postures as relative configuration of rotational joints, expressed using θ_n and utilizing the *Poser* rendering software [23], to derive link configurations from an animated avatar. The approach allowed us to visually inspect and verify link configurations, and manipulate the avatar to match pictures taken during actual posture performances. Fig. 2 illustrates our digitizing and modeling procedure. A normal posture (standing upright, arms down, and elbow and back of the hand laterally aligned to the trunk) was used as reference for modeling all elbow and shoulder exercises.

B. Sensor Model

A sensor modeling was used to derive outputs of arbitrary sensors attached to body segments based on the kinematic body model, according to Fig. 1. This module transforms link orientations, provided in world coordinates, into specific sensor outputs in a local coordinate system. The sensor model can be configured regarding location at body segments and sensor modality. Both are garment design aspects, which are typically defined during prototyping. In this study, we considered the following modalities.

1) *3-D-acceleration:* Acceleration sensors are sufficient for gravity-based detection of various static postures [9]. The sensor output was derived by projecting the body-model orientation vectors along the three axes of a link's local coordinate system onto the z-axis of the world system. A detailed description of the acceleration sensor model was provided in an earlier study [19].
2) *3-D-magnetic field:* Magnetic field sensors are advantageous in static and dynamic applications, in particular to supplement the incomplete orientation information of acceleration sensors. The output for magnetic field sensors was derived in the same way as for acceleration sensors. Unit vectors along a link's local coordinate axes were projected onto the global system's y-axis.

This investigation considered static postures. Nevertheless, the framework could be extended to address dynamic motion. For this purpose, a motion should be generated in the kinematic body model as a chronological variation of link configurations.

IV. GARMENT ERROR MODELING

The body-sensor modeling introduced in Section III provides ideal sensor outputs as they would occur for sensors tightly fixed to the human body. We subsequently introduce a wrinkle-modeling approach (see Fig. 1) to derive orientation errors modulated onto those ideal sensor orientation. Our modeling addresses a local, geometric wrinkle representation as a consequence of BGM. Due to the challenges in garment shape simulation, we focus here on a statistical estimation of orientation errors. Subsequently, terms used to describe orientation errors are introduced, a generalized analytical model for wrinkles that depends on BGM is presented, and the influence of BGM on SOEs is described.

A. Terms Used to Describe Orientation Errors

Body-Garment Mobility (BGM): To derive the wrinkle model, we approximate body segments, including extremities considered in this study, by cylinders. Fig. 3 illustrates a

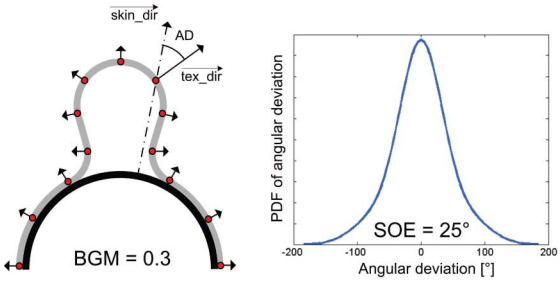

Fig. 3. Left: Illustration of arm cross sections with a potential wrinkle configuration in casual garment with BGM $= 0.3$. Red dots represent potential sensor locations and their normal vectors. Right: Normal vectors of skin and garment describe an AD, quantified in a distribution plot. The SOE is 25°. See Section IV for details.

body-segment cross section embraced by a casual garment with an arbitrary outline. The BGM of this cross section is linked arm and garment geometry. We postulate BGM as a dimensionless ratio between circumferences of garment D_{Garment} and body segment D_{Segment}. At an arbitrary cross-section position

$$\mathrm{BGM} = \frac{D_{\mathrm{Garment}}}{D_{\mathrm{Segment}}} - 1. \tag{1}$$

For tight-fitting garments, circumferences of garment and body segment will be almost identical; hence, BGM $\rightarrow 0$. If garment circumference increases, BGM increases too. According to conversations with designers, convenient casual clothing typically exhibits some "looseness". Using the BGM metric, we expect BGM $\approx 0.1, \ldots, 0.5$ at most body positions. We subsequently consider BGM as the metric describing garment fitting.

Angular Deviation (AD): Angular deviation (AD) denotes the effective deviation of garment and body-segment orientation, and thus is affected by garment fitting and sensor location. For example, body-attached sensors and tight-fitting garments (see Fig. 3) would result in identical directions of normal vectors for sensor and body segment. When BGM increases, garment-attached sensors can vary in orientation, thus normal vectors of sensor and body segments assume different directions. Hence, we define AD as angle between normal vectors of skin- and garment-attached sensors at a specific body position. AD was used in this form in our earlier study [19], and is needed here to formulate the location-independent SOE.

Sensor-Orientation Error (SOE): SOE describes the statistical orientation error between garment-attached sensor and a body segment. While AD depends on the actual position at a body segment cross section, SOE is independent of it.

We derive SOE by estimating AD at equidistant cross-section positions, yielding an AD probability distribution function (PDF). Using kernel density estimation (KDE), we approximate a Gaussian distribution for AD by sampling orientations of a wrinkle surface, corresponding to potential sensor locations. Fig. 3 shows the PDF for AD exemplarily with BGM $= 0.3$. Since the probability for large normal vector deviations increases with wrinkle size, the standard deviation of AD will increase as well. In contrast, tight-fitting garments will exhibit a minimal standard deviation for AD, since AD is zero at all positions. Subsequently, we denote the SOE as standard deviation of AD. The implementation of this approach is detailed in Section IV-C.

B. Generalized Geometric Wrinkle Model

To obtain AD statistics and SOE, a complete description of potential textile orientation in wrinkles is needed. For this purpose, we developed a geometric wrinkle model that approximates the textile shape.

Previous research in the field of drape formation approximated garment wrinkles by symmetric buckling curves [24]. These models have a large number of independent parameters and demand to resolve elliptic integrals. This makes them impractical for extensive simulations. Our modeling approach approximates wrinkles by circles. It allows computational inexpensive simulations of symmetric and asymmetric wrinkles by a minimal set of independent parameters.

Fig. 4 illustrates essential elements of our modeling approach. Two circles serve as textile guide to form configurable wrinkles in two modes. A center circle (CC) determines position and shape of the wrinkle top. A decentered circle (DC) is positioned at the body segment circumference and defines a wrinkle's onset. While the DC circle is always in contact with a body segment in our model, the CC circle can scale in distance to the body segment.

A *symmetric-type* wrinkle is formed, if a wrinkle cross section is rotation-symmetric. Wrinkle geometry can be described by one wrinkle-half in this case. The symmetric-type mimics wrinkles that are formed when zero or negative force is observed at wrinkle top, pointing to the cross section center. Such wrinkles occur naturally, e.g., when a wrinkle pointing in the direction of earth gravitation occurs.

An *asymmetric-type* wrinkle is a "flipped" wrinkle, as illustrated in Fig. 4. This type is frequently observed when positive force is applied to a wrinkle top pointing to the cross section center or if a textile is compressed.

By configuring the two circles, arbitrary wrinkles can be approximated with a set of five parameters:

1) r_a: radius of body segment, e.g., arm (constant);
2) r_{CC}: radius of CC circle;
3) l_{CC}: elevation of CC circle above body segment surface;
4) r_{DC}: radius of DC circle;
5) ω: angle between CC and DC circles.

These five parameter are sufficient to derive both, textile orientation through normal vectors and textile circumference around a body segment. The latter is used in combination with body-segment circumference to determine BGM, according to (1).

The wrinkle shape is derived in closed form by describing sectors that begin and end at CC and DC circles, and body-segment circumference (see Fig. 4). Symmetric-type wrinkles are represented by four individual sectors (S^1–S^4), that are mirrored to represent the complementary half. Asymmetric-type wrinkles form a more complex shape, which can nevertheless

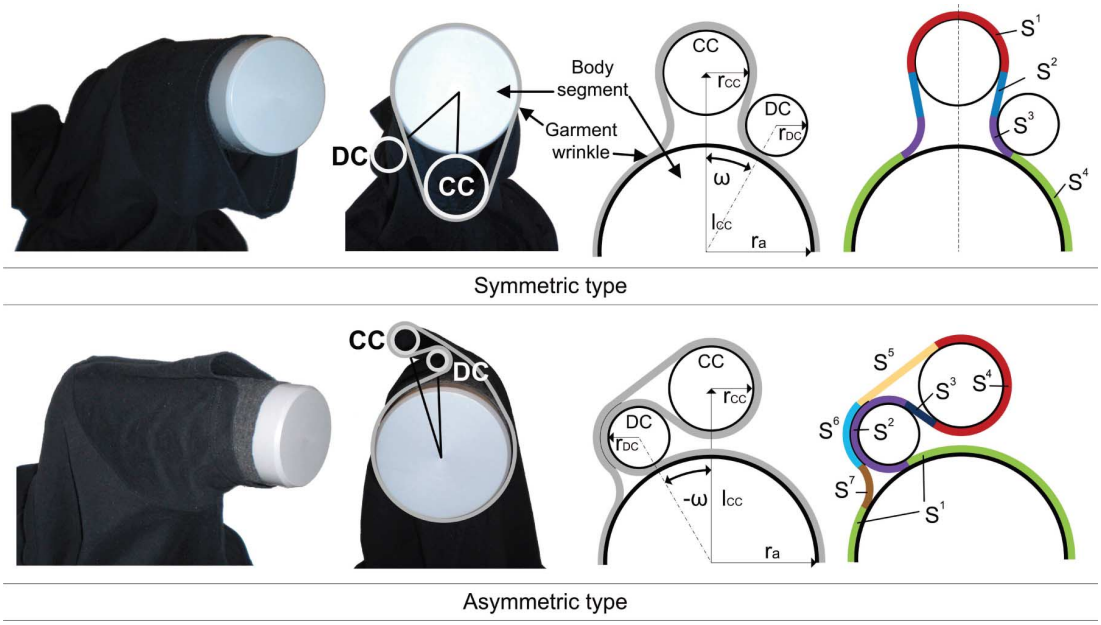

Fig. 4. Illustration of two potential wrinkle configurations. Both wrinkle types are defined by five parameters (ω, l_{CC}, r_{CC}, r_{DC}, r_a) that determine position of two circles determining the wrinkle shape. Symmetric-type wrinkle orientation was described by four sectors (S^1–S^4). For asymmetric-type wrinkles, seven sectors (S^1–S^7) were required.

Algorithm 1 wrinkle_model: Pseudo code to derive AD and BGM from a wrinkle description with sectors S^n

Require: r_a, r_{CC}, r_{DC}, l_{CC}, ω

1: $D_{\mathrm{Garment}} = 0$
2: $D_{\mathrm{Segment}} = 2\pi r_a$
3: $AD = \{\}$
4: **for all** sectors S^n **do**
5: S^n_{start} = [calculate start coordinates of S^n]
6: S^n_{end} = [calculate end coordinates of S^n]
7: S^n_{len} = [calculate length of S^n]
8: **for** sensor position $i = S^n_{\mathrm{start}}$ **to** S^n_{end} **do**
9: tex_dir = [normal vector on textile at i]
10: $skin\_dir$ = [normal vector on skin at i]
11: $\mathrm{ad}^i = tex\_dir - skin\_dir$
12: $AD = \{AD, \mathrm{ad}^i\}$
13: **end for**
14: $D_{\mathrm{Garment}} = D_{\mathrm{Garment}} + S^n_{\mathrm{len}}$
15: **end for**
16: $\mathrm{BGM} = D_{\mathrm{Garment}}/D_{\mathrm{Segment}} - 1$
17: **return** AD, BGM

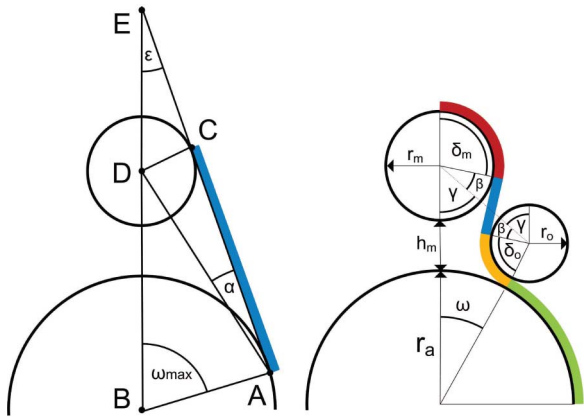

Fig. 5. Left: Illustration of geometric relations to obtain angle ω_{max}. Right: Illustration of all geometric parameters required to derive AD and BGM for sector 1 (S^1) of a symmetric wrinkle.

be fully described by seven sectors (S^1–S^7). Our procedure to calculate ADs is the same for both cases.

C. Estimation of AD and BGM From Wrinkles

The derived wrinkle descriptions were used to represent potential sensor positions at equidistant cross section positions. For each position, textile normal vectors of a wrinkle tex_dir are compared to normal vectors of the underlying skin $skin\_dir$ to compute AD and BGM. Algorithm 1 specifies the procedure based on a sectorwise description S^n.

We detail our approach to obtain a wrinkle description by exemplary discussing all procedural steps for sector 1 (S^1) in a symmetrical-type wrinkle, as illustrated in Fig. 5. Sector S^1 starts at top of CC and follows the CC circumference to angle δ_{CC}. The distance between body-segment center (0,0) and CC (l_{CC}) is given as a simulation parameter, while for DC, $l_{\mathrm{DC}} = r_a + r_{\mathrm{DC}}$. The distance between CC and DC centers (l_x) is obtained according to the cosines law $l_x = \sqrt{{l_{\mathrm{CC}}}^2 + {l_{\mathrm{DC}}}^2 - 2 l_{\mathrm{CC}} l_{\mathrm{DC}} \cos(\omega)}$. These distances are needed to obtain angles of CC, where $\beta = a\cos(\frac{{l_{\mathrm{DC}}}^2 - {l_x}^2 - {l_{\mathrm{CC}}}^2}{-2 l_x l_{\mathrm{CC}}})$, $\gamma = a\cos(\frac{r_{\mathrm{CC}} + r_{\mathrm{DC}}}{l_x})$, $\delta_{\mathrm{CC}} = \pi - (\gamma + \beta)$. This geometric information is sufficient to calculate length, start, and ending coordinates of S^1 in lines 5–7 of Algorithm 1

$$S^1_{\mathrm{start}} = \{0, l_{\mathrm{CC}} + r_{\mathrm{CC}}\} \tag{2}$$

$$S^1_{\mathrm{end}} = \left\{ r_{\mathrm{CC}} \cos\left(\frac{\pi}{2} - \delta_{\mathrm{CC}}\right), l_{\mathrm{CC}} + r_{\mathrm{CC}} \sin\left(\frac{\pi}{2} - \delta_{\mathrm{CC}}\right) \right\} \tag{3}$$

$$S^1_{\mathrm{len}} = 2(\gamma + \beta) r_{\mathrm{CC}}. \tag{4}$$

In (4), a factor 2 is inserted to account for wrinkle symmetry.

Subsequently, the shape of S^1 is sampled to obtain sensor orientations. In our simulations, we defined a sampling interval d to $d = 0.1\,\text{mm}$, as it represents a typical distance between yarns in a fabric. In total, $I = S^1_{\text{len}}/d$ potential sensor positions are considered in S^1; thus, the set of ADs obtained for S^1 is $\text{AD} = \{\text{ad}^1, \ldots, \text{ad}^I\}$. As result, ad^i (line 11 in Algorithm 1) is derived for each sensor position $i = \{1, \ldots, I\}$ at S^1 according to

$$\text{ad}^i = a\text{tan}\left(\frac{r_{\text{CC}}\cos\left((\pi/2) - (\delta_{\text{CC}} i/I)\right)}{l_{\text{CC}} + r_{\text{CC}}\sin\left((\pi/2) - (\delta_{\text{CC}} i/I)\right)}\right) - \left(\frac{\delta_{\text{CC}} i}{I}\right). \tag{5}$$

The terms in (5) corresponds to textile orientation (tex_dir) and skin orientation ($skin\_dir$). To account for a symmetric-type wrinkle, the complementary side is considered by appending negated AD values to our result set obtained: $\text{AD} = \{\text{AD}, -\text{AD}\}$.

Start and end coordinates, length, and AD of all remaining sectors S^2–S^4 for symmetric-type wrinkles, and all seven sectors of asymmetric-type wrinkles were obtained corresponding to this procedure. By summing all sector length results S^n_{len}, a garment's BGM [corresponding to (1)] was obtained

$$\text{BGM} = \left(\frac{1}{2\pi r_a}\sum_n S^n_{\text{len}}\right) - 1. \tag{6}$$

D. Model Boundary Conditions

Specific parameter configurations of the wrinkle model result in undefined model states, such as when textile and body-segment cross section collide, or model sectors become non-continuous due to circle collisions. To resolve collisions, an automatic parameter adaptation for ω and l_{CC} was performed as a function of all remaining parameters r_a, r_{DC}, and r_{CC}. This step is essential to reduce model boundary conditions when performing simulations.

1) Adaptation of ω: Angle ω needs to be constrained to avoid intersection of textile and arm cross section. The boundary condition for $\omega = \omega_{\max}$ is illustrated in Fig. 5. $\omega_{\max}$ occurs, if sector 2 (S^2) connects CC and body segment as tangent with $S^2_{\text{len}} > 0$. As depicted in Fig. 5, section $\overline{CD}$ is given by r_{CC}, $\overline{BD}$ by l_{CC}, and $\overline{AB}$ by r_a. According to the intercept theorem, $\overline{ED}$ was obtained through $\overline{ED} = -r_{\text{CC}} l_{\text{CC}}/(r_{\text{CC}} - r_a)$. $\overline{EC}$ was obtained by trigonometric relations to $\overline{EC} = \cos\left[\arcsin\left(r_{\text{CC}}/\overline{ED}\right)\right]\overline{ED}$. Given $\overline{EC}$ and $\overline{ED}$, α is determined by $\alpha = a\text{tan}\left(r_{\text{CC}}\overline{ED}/\overline{EC} l_{\text{CC}}\right)$, and thus, the maximum angle for ω is

$$\omega_{\max} = a\sin\left(\frac{r_{\text{CC}}\sin(\frac{\pi}{2} - \alpha)}{l_{\text{CC}}\sin(\alpha)}\right). \tag{7}$$

2) Adaptation of l_{CC}: For small ω the distance between CC and DC centers (l_x) could become smaller than $r_{\text{CC}} + r_{\text{DC}}$. Consequently, CC and DC would intersect and wrinkle model sectors become noncontinuous. To avoid this condition, CC is elevated by increasing l_{CC} to the minimal value at which no intersection occurs. For a given parameter set, minimum elevation $l_{\text{CC}'}$ is determined by

$$l_{\text{CC}'} = \frac{r_{\text{DC}} + r_{\text{CC}}}{\sin(\omega)}\sin\left[\pi - \omega - \arcsin\left(\frac{l_{\text{DC}}\sin(\omega)}{r_{\text{DC}} + r_{\text{CC}}}\right)\right]. \tag{8}$$

Algorithm 2 Mapping of SOE and BGM by sweeping the wrinkle model parameters

```
1: ∀BGM : AD(BGM) = {}
2: ∀BGM : SOE(BGM) = {}
3: for all r_CC, r_DC, l_CC and ω do
4:    AD_temp = [get AD from Algorithm 1]
5:    BGM = [get BGM from Algorithm 1]
6:    AD(BGM) = {AD(BGM), AD_temp}
7: end for
8: for all BGM do
9:    AD(BGM) = [KDE of AD(BGM)]
10:   SOE(BGM) = [STD of AD(BGM)]
11: end for
12: return SOE(BGM)
```

E. Estimating SOE for Given BGM

The geometric wrinkle model allows inference of AD and BGM from specific wrinkles according to Algorithm 1. However, this algorithm does not reveal information about AD for wrinkles that can emerge at a given BGM. In this section, we illustrate the relation between SOE and BGM for a generic parameter set of our wrinkle model.

To derive a SOE-BGM mapping, we swept wrinkle model parameters in a specified range. For all resulting wrinkle implementations, we calculated AD and BGM. In our simulation, we addressed the following parameter space:

1) r_a: is constant (e.g., 60 mm);
2) r_{CC}: 1 mm to $r_a/2$ in steps of 1 mm;
3) l_{CC}: $r_{\text{CC}} + r_a$ to $r_{\text{CC}} + r_a + r_a/2$ in steps of 1 mm;
4) r_{DC}: 1 mm to $r_a/2$ in steps of 1 ;
5) ω: $\omega_{\max}$ to $-\omega_{\max}$ in steps of -1°.

Resulting wrinkles outside a range of $0 \leq \text{BGM} \leq 0.8$ were neglected, since $\text{BGM} < 0$ is not feasible and $\text{BGM} > 0.8$ is impractical for conventional garments.

Algorithm 2 was used to analyze our parameter space and estimate SOE from BGM. The parameter sweep resulted in 1 018 195 valid, unique wrinkle descriptions. For each wrinkle, this algorithm assigns AD (AD_{temp}) from Algorithm 1 to a set of ADs for wrinkles of a particular BGM (AD(BGM)). In a subsequent step, the AD(BGM) set was used for a KDE with a Gaussian kernel [25]. Finally, we calculated SOE as standard deviation of obtained AD distributions. Since the expected value of AD is $E[\text{AD}] = 0$, the standard deviation is simplified to

$$\text{SOE}(\text{BGM}) = \sqrt{\frac{1}{|\text{AD}(\text{BGM})|}\sum_{\text{BGM}} \text{AD}(\text{BGM})^2}. \tag{9}$$

F. Evaluation of the Garment Model

Fig. 6 shows that sensor mobility and SOE are increasing with BGM.

For $\text{BGM} = 0$, which represents a tight-fitting garment, SOE is 0°, as expected. For casual garments, a $\text{BGM} = 0.2$ can be

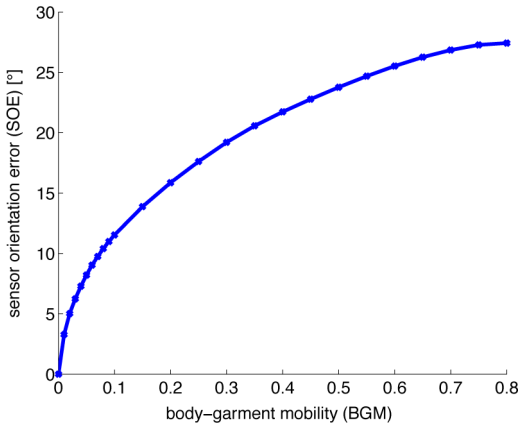

Fig. 6. SOE with respect to BGM as simulated with the geometric wrinkle model.

expected at forearm and upper arm. For this BGM, a SOE of 15.5°is predicted by the model.

V. Framework Validation

We validated our framework by comparing estimated recognition performance between simulation and an experimental study using the SMASH prototyping garment [3].

In particular, we targeted to analyze effects of different BGM settings on SOE and the final posture-recognition performance for rehabilitation exercise postures.

A. Experimental Study Methodology

We asked five healthy volunteers to perform a set of shoulder rehabilitation exercises including ten postures, as illustrated in Fig. 8. Each posture was adopted for ∼3 s followed by a normal posture (see posture 1 in Fig. 8) to realign the garment and prepare for subsequent postures. The complete exercise set was repeated for three times. During recordings, the garment was not manually realigned. The posture set was specified by rehabilitation experts, as it is used in movement rehabilitation to train shoulder and elbow functions.

Study participants wore a SMASH prototyping garment [3]. SMASH is a rapid prototyping architecture that has been specifically designed to study sensing and processing functions of smart garments. It comprises a garment-embedded distributed processing network and sensing/actuation elements that can be flexibly configured.

In this study, 3-D-acceleration sensors were attached to the forearm and upper arm (see Fig. 7). Sensor data was continuously streamed using a Bluetooth link from SMASH to a recording PC. In a postprocessing step, acquired data were inspected and annotations obtained during study recordings were refined.

One SMASH garment in size "large" was used and kept for recordings with all participants. Four participants were selected to include different body proportions and varying BGM values. BGM figures were derived from circumference measurements of each participant and the SMASH garment used [according to (1)]. For the fifth participant, sensors were fixed onto skin to evaluate the effect of an ideal tight-fitting garment, thus resulting in a BGM of zero. Table II summarizes the participant data of our validation study.

Fig. 7. (a) Inner side of the SMASH prototyping garment, including a hierarchical sensing and processing architecture. (b) Sensor positioning at the forearm and upper arm (encircled) used for model and simulation validation.

TABLE II
Validation Study Participant Data and Recognition Performances

Participant data			Measured BGM		Accuracy [%]	
#	sex, height	fit	u.arm	f.arm	simulation	exp. study
1	m, 190cm	t	0.03	0.15	93	98
2	m, 182cm	i	0.27	0.37	84	85
3	m, 173cm	(i)	0.1	0.4	86	94
4	f, 163cm	l	0.3	0.65	79	75
5	m, 182cm	s	0	0	100	100

Fit indicator definitions: s = skin-attached (BGM = 0), t = tight (0 < BGM ≤ 0.2), i = ideal (0.2 < BGM ≤ 0.4), l = loose (0.4 < BGM ≤ 1)[a].

[a] BGM ranges serve as approximate indications of perceived fitting. Ideal fit corresponds to garment manufacturer's sizing guidelines.

Performance evaluation: To derive posture-recognition performance, a nearest centroid classifier (NCC) was deployed for both, experimental data and the framework-simulation output. The NCC was trained with sensor data (simulated or recorded) as features. Classification performance was analyzed in a threefold cross-validation scheme, where each two of all three exercise iterations were used for training, and testing was performed on the remaining set. Each exercise repetition was used once for testing. The final accuracy was determined as average of individual cross-validation results.

B. Framework Configuration

Our framework was configured according to used postures, sensors, and BGM of the validation study. We summarize our steps to obtain configuration data in this section.

Configuration of the kinematic body model: Reference photographs were taken from all study postures. These served as modeling reference to obtain link configurations for the body model as described in Section III. Rendered representation of the postures are depicted in Fig. 8, respective link configurations are summarized in Table III.

Configuration of the sensor simulation model: Using the kinematic body-model output, 3-D-acceleration sensors and their positions at forearm (at the wrist) and upper arm (at the deltoid muscle onset) were simulated.

Configuration of the garment error model: Each sensor and sensor axis of our sensor simulation model output was superimposed with a Gaussian distribution of zero mean and a standard deviation corresponding to our estimated SOE. In particular,

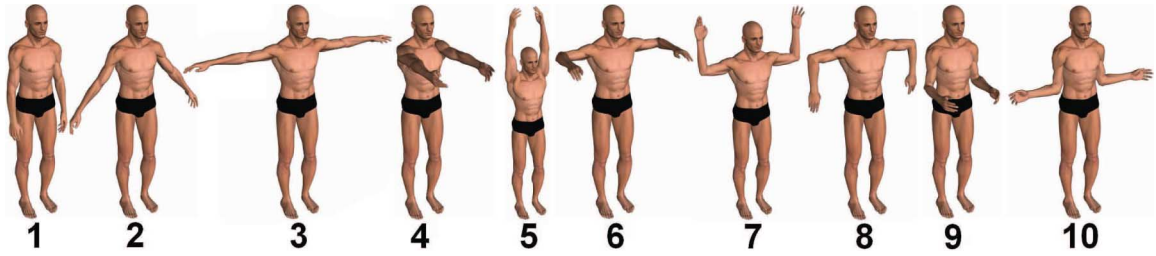

Fig. 8. Illustration of shoulder rehabilitation exercise postures used in validation and exploratory analyses. Postures were modeled for the kinematic body model according to Section III. The resulting link configurations are listed in Table III.

TABLE III
LINK CONFIGURATIONS FOR ALL SIMULATED REHABILITATION POSTURES (AS ILLUSTRATED IN FIG. 8)

Posture #	Should. exten. [°]	Should. abduc. [°]	Should. int. rot. [°]	Elbow flex. [°]	F.arm pron. [°]
1	0	15	70	10	15
2	0	40	90	0	90
3	0	90	-100	0	100
4	80	90	-90	10	0
5	0	180	-180	0	0
6	0	90	-90	90	90
7	0	90	-180	-90	90
8	0	90	0	90	90
9	0	15	-90	90	90
10	0	15	-180	80	90

SOE was estimated according to the simulation results derived in Section IV, as shown in Fig. 6.

BGM of forearm and upper arm were individually adjusted according to participant-specific parameters (see Table II). As these BGM figures indicate, participants fitted the garment in a wide range of $0 \leq \text{BGM} \leq 0.65$. To provide a semantic interpretation, we partitioned BGM ranges into tight, ideal, and loose.

C. Validation Results

Table II shows the recognition performances as predicted by simulation and obtained from study data. Our evaluation of participant #5 showed that when skin-attached sensors were used (BGM $= 0$), simulation predicted a perfect posture classification accuracy. This result was closely achieved with our study data as well, which confirmed that our considered rehabilitation postures can be well discriminated with the chosen configuration.

Body height of participant #2 matched SMASH according to the garment manufacturer's sizing guide. Participant #3 fitted the garment similarly regarding BGM, nevertheless, participant #2 was lean compared to #3. Our simulation predicted accuracies of 84% for participant #2 and 86% for #3, while study data yielded 85% for #2 and 94% for #3. This result confirms that body proportions determine sensor mobility and influence recognition performance. Height seems to be less relevant.

Participant #1 was subjectively too large for the selected SMASH garment. Both, simulation framework performance prediction (93%) as well as that from study data (98%) confirmed that the garment incurs only small performance drops compared to skin-attached sensors. Participant #4 was too small to fit SMASH, thus resulting in a loose fit. Recognition accuracy of 79% for simulation overestimated our experiment slightly (75%). Visual inspection of garment sleeves confirmed extensive compressions and shifts at wrist region where one sensor was attached.

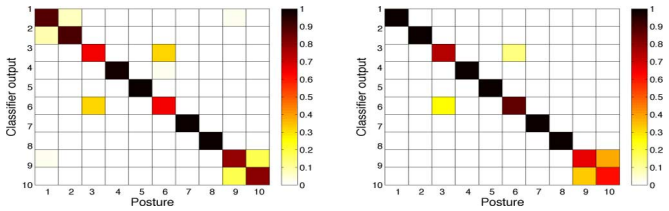

Fig. 9. Posture classification confusion matrices for participant #2 to assess misclassified postures. (a) Framework simulation. (b) Experimental study data.

An essential point of interest during garment prototyping is *a priori* information on potentially misclassified postures. Early evaluations of potential errors could be performed by analyzing confusion matrices derived from classifier outputs. Fig. 9 shows confusion matrices for simulated and study sensor data from participant #2. The simulation result in Fig. 9 indicates minor confusion of postures (1,2) and further confusions for postures (3,6) and (9,10). Although the result matrix obtained for study data showed no confusion for postures (1,2), it reveals similar results for (3,6) and (9,10). A congruence between simulation and study data was obtained for participants #1 and #3. For participant #4, different confusions were found, which we attributed to the loose-fit condition and resulting randomness in SOE for this case.

We concluded that framework predictions of posture-discrimination performance matched well with validation study results. The mean difference between predicted recognition performances and results from validation trials was below 4%.

VI. EXPLORATORY PERFORMANCE ANALYSIS

Our simulation framework can be used to investigate effects of garment fitting, sensor modalities, and sensor position on posture-recognition performance before implementing garment prototypes. We exemplarily analyze the impact of garment fitting and benefits of additional sensor modalities in this section.

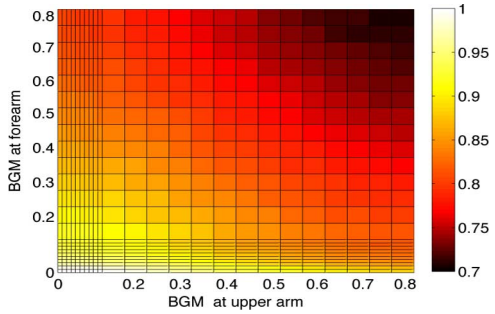

Fig. 10. Simulated recognition performance of rehabilitation postures (see Fig. 8) regarding BGM for acceleration sensors at forearm and upper arm.

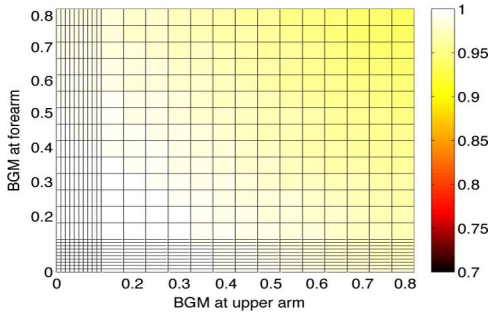

Fig. 11. Simulated recognition performance regarding BGM for a combination of acceleration and magnetic field sensors at forearm and upper arm.

A. *Impact of Garment Fit (BGM) on Recognition Performance*

To investigate effects of garment-induced errors on recognition performance of rehabilitation postures depicted in Fig. 8, we evaluated BGM in the parameter space $0 \leq \text{BGM} \leq 0.8$. For this simulation, NCC class centroids were trained by noise-free sensor data; thus; no SOE was modulated onto training sensor data. Classification performance was evaluated with 1500 test samples that were modulated with a Gaussian-sampled SOE corresponding to a particular BGM. All other framework configurations and our evaluation methodology were kept constant, as detailed in Section V.

We derived sensor outputs for forearm and upper arm independently. Fig. 10 shows a simulated classification performance map for both sensor positions. The color-coded classification performance confirms its dependency on SOE and consequently on garment fitting. For a tight fit ($\text{BGM} = 0$) at forearm and upper arm, a perfect discrimination is achieved. For our configured posture set, performance remains perfect when the forearm sensor remains tight fitted and BGM at the upper arm is increased up to 0.15. Hence, in this configuration, tight alignment of a garment at the forearm is crucial, while non-tight fit can be tolerated at the upper arm.

We observed that convenient clothing typically exhibits a BGM of $\sim$0.2 at the upper arm, and $\sim$0.3 at the lower arm. For this case and our analysis configuration (rehabilitation postures and sensors), a classification accuracy of 85% is predicted.

B. *Impact of Sensing Modalities*

Fig. 9 indicates that classifier confusions occur due to incomplete orientation information as provided by static acceleration sensing. Specifically, postures (3,6) and (9,10), that were confused, differ predominantly in body-segment rotation around the gravity vector. Since this information cannot be captured by acceleration sensors, additional sensor modalities could be considered to resolve these misclassifications. We analyzed potential benefits of additional magnetic field sensors to supplement acceleration readings. The complementary information of these two modalities provides complete orientation information in static situations, thus potentially resolve confusions and increase robustness against orientation errors.

The sensor simulation model was reconfigured to include 3-D magnetic field sensing instances at forearm and upper arm. Fig. 11 shows a simulated classification performance map for this configuration. Our result indicated that an almost perfect discrimination of all postures (>98%) can be achieved for BGM values up to $\sim$0.4 at the upper arm and forearm.

These exploratory results for using additional magnetic field sensors indicated that for all study participants considered in Section V, a recognition of >97% would be achieved. This result suggests that an additional selected sensor modality can lead to profound performance improvements, also for casual clothing. The average recognition performance of participants #1–4 would be increased by $\sim$12% to $\sim$97.5% for this situation.

VII. Conclusion

In this study, we introduced a framework to simulate garment-based SOEs depending on BGM. Validation of our simulation framework with experimentally derived recognition performances in a set of rehabilitation exercise postures confirmed congruent performance trends with errors below 4% for all study participants. In addition, similar confusion matrices were observed for four out of five participants. We concluded that our simulation approach is adequate to be utilized in performance prediction related to garment fitting and estimation of posture confusion.

Moreover, our framework enables us to analyze benefits of using alternative or complementary sensor modalities in specific BGM settings. Simulation of complementary magnetic field sensors increased recognition performance by $\sim$12% for rehabilitation exercises considered in this study. From these results, we concluded that a combination of acceleration and magnetic field sensors could compensate recognition errors for settings with larger BGM. Thus, setups with extended, specifically selected sensors could enable robust garment operation at reduced constraints on tight garment fitting.

We showed how our framework can become a valuable tool during rapid prototyping of smart garments: it allows evaluating design options before implementing them into garments and performing participant evaluation studies. Further work is needed to address additional sources of BGM, regarding propagated garment strain and dynamic movements. We expect that our framework could be extended to address these challenges.

ACKNOWLEDGMENT

The authors would like to thank the participants of the rehabilitation exercise study considered in this study, and C. Schuster, MPTSc, and R. Rheinfelden, for revising the rehabilitation exercises and notation used in this study.

REFERENCES

[1] H. Zheng, N. Black, and N. Harris, "Position-sensing technologies for movement analysis in stroke rehabilitation," *Med. Biol. Eng. Comput.*, vol. 43, no. 4, pp. 413–420, 2005.

[2] M. Sung, C. Marci, and A. Pentland, "Wearable feedback systems for rehabilitation," *J. Neuroeng. Rehabil.*, vol. 2, no. 1, p. 17, 2005.

[3] H. Harms, O. Amft, D. Roggen, and G. Tröster, "Rapid prototyping of smart garments for activity-aware applications," *J. Ambient Intell. Smart Environ.*, vol. 1, no. 2, pp. 87–101, 2009.

[4] R. Paradiso, C. Belloc, G. Loriga, and N. Taccini, "Wearable healthcare systems, new frontiers of e-textile." in *Personalised Health Management Systems: The Integration of Innovative Sensing, Textile, Information and Communication Technologies* (Studies in Health Technology and Informatics series), vol. 117, Amsterdam, The Netherlands: IOS Press, 2005, pp. 9–16.

[5] A. Lymberis and S. Olsson, "Intelligent biomedical clothing for personal health and disease management: State of the art and future vision," *Telemed. J. E-Health*, vol. 9, no. 4, pp. 379–386, 2003.

[6] S. Coyle, D. Morris, K.-T. Lau, D. Diamond, and N. Moyna, "Textile-based wearable sensors for assisting sports performance," in *Proc. 6th Int. Workshop Wearable and Implantable Body Sensor Netw.*, Washington, DC, 2009, pp. 307–311.

[7] W. Wong and M. Wong, "Detecting spinal posture change in sitting positions with tri-axial accelerometers," *Gait Posture*, vol. 27, no. 1, pp. 168–171, 2008.

[8] H. Harms, O. Amft, M. Appert, R. Muller, and G. Tröster, "Wearable therapist: Sensing garments for supporting children improve posture," in *Proc. 11th Int. Conf. Ubiquitous Compu.*, New York, 2009, pp. 85–88.

[9] H. Harms, O. Amft, and G. Tröster, "Influence of a loose-fitting sensing garment on posture recognition in rehabilitation," in *Proc. Biomed. Circuits and Syst. Conf.*, Piscataway, NJ, Nov. 2008, pp. 353–356.

[10] A. Tognetti, F. Lorussi, R. Bartalesi, S. Quaglini, M. Tesconi, G. Zupone, and D. De Rossi, "Wearable kinesthetic system for capturing and classifying upper limb gesture in post-stroke rehabilitation," *J. Neuroeng. Rehabil.*, vol. 2, no. 1, p. 8, Mar. 2005.

[11] C. Mattmann, O. Amft, H. Harms, C. Tröster, and F. Clemens, "Recognizing upper body postures using textile strain sensors," in *Proc. 11th IEEE Int. Symp. Wearable Comput.*, Piscataway, NJ, Oct. 2007, pp. 29–36.

[12] O. Amft, H. Harms, G. Troester, and C. Schuster, "Estimating exercise execution quality from garment-integrated sensors," *Neurorehabil. Neural Repair*, vol. 22, no. 5, p. 616, 2008.

[13] K. Kunze and P. Lukowicz, "Dealing with sensor displacement in motion-based onbody activity recognition systems," in *Proc. 10th Int. Conf. Ubiquitous comput.*, New York, 2008, pp. 20–29.

[14] P. Zappi, T. Stiefmeier, E. Farella, D. Roggen, L. Benini, and G. Tröster, "Activity recognition from on-body sensors by classifier fusion: sensor scalability and robustness," in *Proc. 3rd Int. Conf. Intell. Sens., Sens. Netw. Inf., 2007* (*ISSNIP 2007*), Dec., pp. 281–286.

[15] D. E. Breen, D. H. House, and J. M. Wozny, "A particle-based model for simulating the draping behavior of woven cloth," *Textile Res. J.*, vol. 64, no. 11, pp. 663–685, 1992.

[16] P. Volino and N. Magnenat-Thalmann, "Accurate garment prototyping and simulation," *Comput.-Aided Design Appl.*, vol. 2, no. 1–4, pp. 645–654, 2005.

[17] J. Hu and Y. Chan, "Effect of fabric mechanical properties on drape," *Textile Res. J.*, vol. 68, no. 1, pp. 57–64, 1998.

[18] D. Lojen and S. Jevsnik, "Some aspects of fabric drape," *Fibres Textiles Eastern Eur.*, vol. 15, no. 4, pp. 39–45, Dec. 2007.

[19] H. Harms, O. Amft, and G. Tröster, "Modeling and simulation of sensor orientation errors in garments," presented at the 4th Int. Conf. Body Area Netw., Los Angeles, CA, 2009..

[20] T. Barker, C. Kirtley, and J. Ratanapinunchai, "Calculation of multi-segment rigid body joint dynamics using matlab," in *Proc. Inst. Mech. Eng., Part H, J. Eng. Med.*, 01 1997, pp. 483–487.

[21] J. Denavit and R. S. Hartenberg, "A kinematic notation for lower-pair mechanisms based on matrices," *Trans. ASME J. Appl. Mech*, vol. 23, pp. 215–221, 1955.

[22] A. Tilley, *The Measure of Man and Woman : Human Factors in Design*, 1st ed. New York: Whitney Library of Design, 1993.

[23] mysmithmicro. (2010). "Poser 6," [Online]. Available: http://my.smithmicro.com/win/poser/index.html.

[24] X. Dai, T. Furukawa, S. Mitsui, M. Takatera, and Y. Shimizu, "Drape formation based on geometric constraints and its application to skirt modelling," *Sci. Technol.*, vol. 13, no. 1, pp. 23–37, 2001.

[25] A. Bowman and A. Azzalini, *Applied Smoothing Techniques for Data Analysis: The Kernel Approach With S-Plus Illustrations*. New York: Oxford Univ. Press, 1997.

Holger Harms received the Dipl.-Ing. degree in information technology from the University of Rostock, Germany, in 2004. Since 2006, he has been working toward the Ph.D. degree at the Wearable Computing Laboratory, ETH Zürich, Zürich, Switzerland.

He completed one semester of traineeship at IBM, Tucson, AZ, and two years in the core development of former Siemens VDO, Germany. His research interests include garment-based sensing of motions in sports and rehabilitation.

Oliver Amft received the M.Sc. degree from Chemnitz Technical University, Germany, in 1999 and the Dr.Sc. ETH (Ph.D.) degree from ETH Zürich, Zürich, Switzerland, in 2008.

Between 2000 and 2004, he lead R&D actives on utility communication systems with ABB Switzerland. He is currently an Assistant Professor at Technische Universiteit (TU) Eindhoven, The Netherlands, and a Senior Research Advisor at Wearable Computing Lab., ETH Zürich. He leads the Activity and Context Technologies Laboratory (ACTLab, www.actlab.ele.tue.nl), Signal Processing Systems, TU Eindhoven. His research interests are in fundamental principles and algorithms for activity recognition and behavior inference with applications in personal healthcare.

Gerhard Tröster (SM'93) received the Dipl.-Ing. degree in electrical engineering from Darmstadt and Karlsruhe, in 1979, and the Dr.-Ing. degree from the Technical University Darmstadt, Darmstadt, Germany, in 1984.

He was involved in the research on design methods of analog/digital systems in CMOS and BiCMOS technology for eight years at Telefunken (atmel), Heilbronn. Since 1993, he has been a Full Professor of electronics at ETH Zürich, heading the Electronics Laboratory. At ETH, he established the multichip module (MCM) electronic packaging group. One of his achievements, the world smallest GPS receiver has lead to the foundation of the spin-off u-blox AG, now world market leader in GPS modules. In 2000, he constituted the Wearable Computing Laboratory, ETH, where he was involved in interdisciplinary approach combining IT, signal processing, electronic platforms, wireless sensor networks, smart textiles, and human-computer interaction. The group aims at methods, technologies, and system platforms for the detection of the physical, mental, and social context of the user.